

How the lockdown affected my project

My project plan, as stated in the project report submitted in December, was to design and build a new version of the prototype muon tomography scanner. I would then be able to assess the effectiveness of my new design experimentally. For example, I had to redesign the cooling system and so a method of assessing the performance would be to monitor its ability to maintain the temperature of the modules within the acceptable region. Time allowing, I also planned to take some preliminary data to perform some calibration of the detector. This was a highly experimental plan.

Due to the COVID 19 outbreak and the subsequent lockdown, the design that I commissioned from the workshop was interrupted and didn't arrive. Without access to the lab I was unable to continue any experimental work on the existing scanner. This essentially put a stop to my entire project. There was no way for me to continue my initial plan in any way.

This forced me to come up with an essentially new project plan which was somewhat achievable in the few months before the deadline. I have had to shift my focus to a computational analysis. To remain in the spirit of my project, I decided to modify the analysis code that could then be used when the scanner is assembled. It then became apparent that there was no good way to test the effectiveness of my modifications with the data available and so I would also have to simulate some data to pass through it.

Fortunately, a Geant4 description of the old detector already existed I 'just' had to modify it to the new setup. Without prior experience with the software a significant portion of time was spent understand the existing setup. I was fortunate enough to have communications via email with the author. He was usually able to answer my questions through a series of emails over the course of a week. Updates out of my control also interrupted my work on numerous occasions. These issues also required inside knowledge to resolve which was obtained via email over the course of a few days thanks to Dr. Wotton. These and similar issues were exacerbated by the lockdown as I was unable to knock on someone's door to ask for help, so problems that might have taken an hour to fix in person took a few days of email exchange.

Furthermore, to use the software, I had to connect to the PC in the lab. Problems with the graphical interface forwarding to my laptop meant I ended up using an Intel NUC with a Linux operating system. This reduced the framerate of the simulation interface to 4fps. Even without the visual interface the simulation of data took around 40 hours to generate, and a further 5 hours to process. This was significantly longer than anticipated. Due to the restricted time frame this meant I could only run the simulation once.

Because of the lockdown, I was unable to satisfactorily complete the study of simulating the data. However, I feel it is important to discuss what I did achieve in the time and so it has been included in the report.



Modification of a prototype muon scattering tomography scanner

University of Cambridge

May 18, 2020

Candidate Number: 8227S

Supervisor: Dr. Christopher Lester

Abstract

Designs for a modification of the prototype Muon Tomography Scanner built by a team at the Cavendish was developed. This modification increased the sample length imageable by the detector from 10cm to 100cm. A new mechanical support and cooling system was designed and commissioned. The analysis software was modified to accommodate for the new geometry. A simulation of the was created to model the passage of cosmic muons through this new geometry and generate the data the scanner would produce. The simulation was performed and analysed in the absence of a sample. The scattering angle displayed a Gaussian distribution with a mean of 1.147mrad and one standard deviation of 2.3mrad. The distribution of the error in the gradient of the muon tracks displayed an expected form with a mode of less than 1mrad. A simulation was also run with the sample present with a run time of 40 hours compared to the 10 hour runtime without a sample. Significantly fewer scattering events were recorded and a image was not reconstructed. A deviation from the Gaussian distribution of scattering angles was observed which is attributed to the presence of a sample

Contents

1 Acknowledgements	2
2 Introduction	3
3 Theory	3
3.1 Cosmic Muons	3
3.2 Multiple Scattering	4
3.3 Experimental Setup	5
3.4 Reconstruction Techniques	7
4 Scanner redesign	8
4.1 Mechanical Support	8
4.2 Light tight Environment	9
4.3 Internal wiring	9
5 Simulation and Analysis	11
5.1 Geant4 detector description	11
5.2 Scattering angle resolution	12
5.3 Image reconstruction	13
6 Conclusion	15
7 References	16
8 Appendix	18
8.1 Technical Drawing of Base Plate	18
8.2 Technical Drawing of Tension Bar	19
8.3 Technical Drawings of Cooling Channel	20
8.4 Simulation with some trajectories displayed	21

1 Acknowledgements

Firstly I would like to thank Chris Burling from the Cavendish Workshop who suggested the use of Aluminium tooling plate as a suitable material and who worked on the manufacture of the mechanical support pieces.

I would also thank Dr Stephen Wotton with whom I shared a lab. Without his guidance I would not have been able to understand the scanner in the level of detail I needed. He was also invaluable during the lockdown bug fixing through email, without which I wouldn't have been able to complete my report.

I based a lot of the work of this project on that of the existing prototype scanner which was written up in detail by Dr Floris Keizer in his PhD. I'd like to thank Floris for letting me use and adapt the software that he created with the help of others and for the supporting information he provided.

Finally I'd like to thank my supervisor Dr Chris Lester for helping me secure a much needed project extension allowing me time to generate some results. Also for the support he has provided throughout the project, especially when the lockdown was implemented and my project had to be reworked.

2 Introduction

Computed Muon Scattering Tomography (MST) is proposed to provide a non destructive method of imaging the internal structure of composite objects with sharp density contrasts. Using naturally occurring cosmic muons as probes, MST avoids the occupational hazards of similar X-ray techniques. It is proposed that this can be used to scan large structures, such as motorway bridges, historic buildings and so forth, potentially saving the maintainers a large amount of money. It has also been proposed to detect high density fissile material in vehicles at borders [1] [2].

A prototype of such a scanner has been built by a team in The Cavendish, using sensors designed for use on the ATLAS particle collider experiment to track the muon entry and exit path [3] [4]. This method of tracking means the scanner can be made mobile, which is desirable over a static drift chamber setup [5]. Using sensors designed for ATLAS also removes the need to manufacture a bespoke sensor, reducing cost.

This report outlines the modifications made to the design of this prototype to accommodate an imaging sample of length 100cm along the axis of the scanner. The maximum imaging width is limited by that of the sensors. At these distances the muons will undergo significant multiple scattering events between the detectors much more frequently than in the existing set up. This will allow a better performance analysis of the reconstruction algorithm, and give an idea of the effectiveness of this technique on the larger, architectural, scales proposed.

Due to the unprecedented situation caused by the COVID-19 pandemic, manufacture of mechanical support structure was interrupted and access to the scanner and lab was removed. Therefore, the second half of this report describes a computational analysis of the long-baseline geometry. A simulation created to model the passage of muons through the new scanner geometry, emulating the data the scanner would produce. This data is then briefly analysed.

The rest of the report will be structured as follows. A discussion of the theory behind the MST technique used will be conducted in Section [3]. An overview of the redesigns created for the long baseline arrangement, the current condition of the MST scanner and a suggestion of future action required for implementation of the new set-up is provided in Section [4]. Section [5] contains the details of the simulation and the respective results. Finally a summary of the outcomes of the project is presented in the conclusion, Section [6].

3 Theory

3.1 Cosmic Muons

Cosmic radiation incident on the Earth's atmosphere is generated by astrophysical sources primarily from outside the Solar System, excluding any contribution from solar flares. A cascade of 'secondary' particles is produced, as interactions with Earth's atmosphere cause the primary particles to decay. Belonging to the set particles abundant in these cascades are charged mesons. These mesons have short lifetimes, therefore will also decay in the atmosphere. One of their decay products are muons, which have a sufficient lifetime ($2.2\mu s$) to reach the Earth's surface [6]. These highly penetrating muons can be used in scattering experiments, without the need for a particle accelerator.

As the muons travel through the atmosphere they lose energy to ionisation and decays. Their

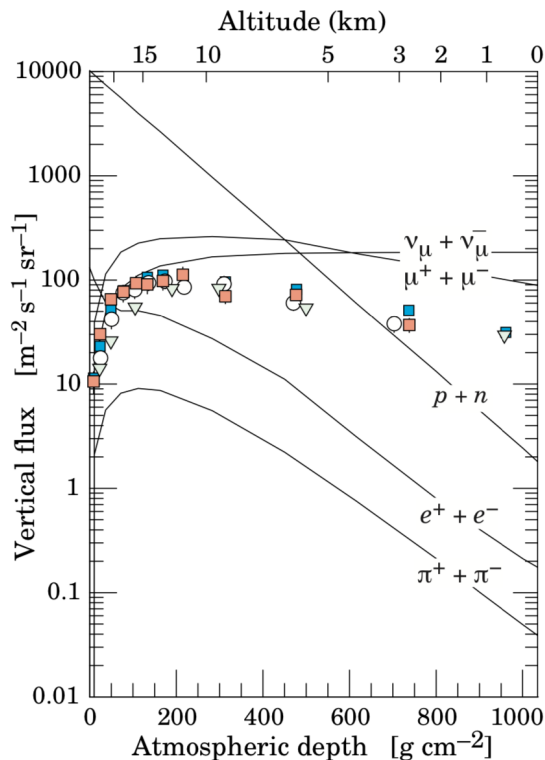


Figure 1: Estimate of vertical fluxes of cosmic rays in the atmosphere with $E > 1\text{GeV}$. The points show measurements of negative muons with $E_\mu > 1\text{GeV}$ [7].

mean energy and flux therefore depends on the distance they travelled through the atmosphere and subsequently depends on their angle of incidence θ . Angle θ is taken with respect to the normal of the Earth's surface (the zenith). The cosmic muons typically reach the surface with an energy of $\approx 4\text{GeV}$ and have a $\cos^2 \theta$ flux dependence [7].

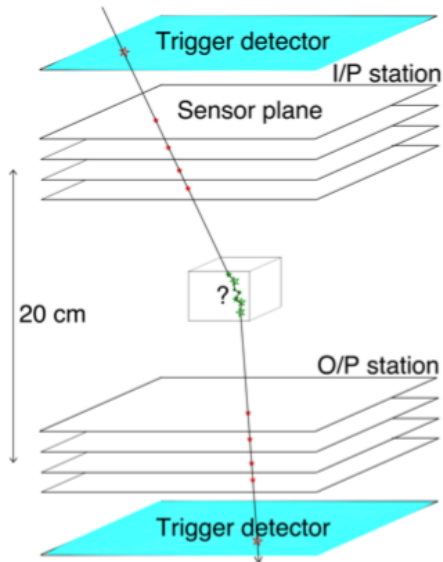
Muons are chosen as a probe, over say electrons, because they are the most numerous charged particle in these cascades at the Earth's surface. Uncharged neutrinos are more abundant but do not leave tracks in the detector and so are not useful. The average flux of muons at the surface is $\approx 1\text{min}^{-1}\text{cm}^{-2}$ as can be seen in Fig. 1. This flux is low, compared to say a conventional X-ray source, so an image produced by MST requires relatively long recording times. The resolution and contrast of the image is dependant on the number of incident muons, thus any decrease in image capture time reduces the quality of the produced image.

3.2 Multiple Scattering

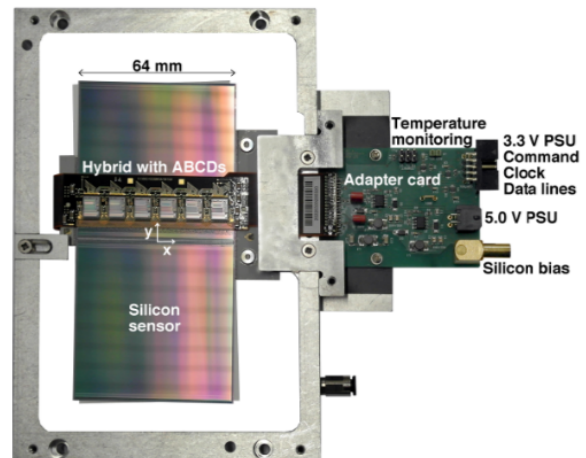
Muons travelling through matter experience the electric potentials of the atoms in that matter and so undergo multiple Coulomb scattering. The subsequent deflection angle will depend on the density and atomic number of the matter. It will also depend on the path length, the distance travelled through the medium, and momentum of the muon. This type of scattering is described by Molière's multiple scattering theory, where the central 98% of the scattering angle distribution is approximately Gaussian [8] with a standard deviation given by

$$\theta_0 = \frac{z \cdot 13.6 \text{ MeV}}{p\beta c} \sqrt{\frac{x}{X_0}} \left[1 + 0.038 \ln \left(\frac{x}{X_0} \right) \right]. \quad (1)$$

Here, p and βc are the momentum and velocity of the muon, $z = 1$ is the charge number of the muon and x and X_0 are the thickness and radiation length of the object respectively. The width



(a) A schematic of an experiment designed to perform muon scattering tomography.



(b) An ATLAS Semiconductor Tracker module mounted on an aluminium handling frame with the adapter card.

Figure 2

of the Gaussian is inversely proportional to the muon's momentum, and inversely proportional to the square root of the radiation length [9] [10]. Radiation length is given by the formula,

$$X_0 = \left[\frac{A \cdot 716.4 \text{ gcm}^{-2}}{Z(Z+1) \ln\left(\frac{287}{\sqrt{Z}}\right)} \right] \left[\frac{1}{\rho} \right] \quad (2)$$

Here, ρ , A and Z are the density, atomic weight and atomic number of the material respectively. The approximate $\frac{1}{\rho Z^2}$ dependence of the radiation length for large Z characterises the sensitivity to dense objects with a high atomic number. This allows the MST scanner to have a high resolution of the density distribution of the matter with high Z , given sufficient sensor resolution.

3.3 Experimental Setup

In Muon Scattering Tomography (MST) experiments, an imaging object is placed between two tracking stations. When cosmic muons are used as a source the stations are placed above and below the sample. These tracking stations consist of several silicon planes normal to the axis of the scanner, Fig. 2a. They detect individual muons entering and leaving the object, recording the position in each plane where the muon passed. From this information the muon's initial and final trajectory is recovered, which is used to obtain the angle through which it was scattered. The experimental setup used in the preexisting prototype scanner is described in further technical detail in [3], in particular the information on the readout boards and triggering system. The information most relevant to this project has been included in this report.

The ATLAS Semiconductor Tracker module shown in Fig. 2b consists of two layers of single-sided p-in-n silicon sensors. Each layer consists of 768 strips with $80\mu\text{m}$ pitch, mounted back-to-back on a thermal conductor. The layers are at a stereo angle of $\pm 20\text{mrad}$, giving position information in the y-direction. The active area of each sensor is $128 \times 64\text{mm}$. To keep scattering in the tracking station, which would reduce the accuracy of the track reconstruction,

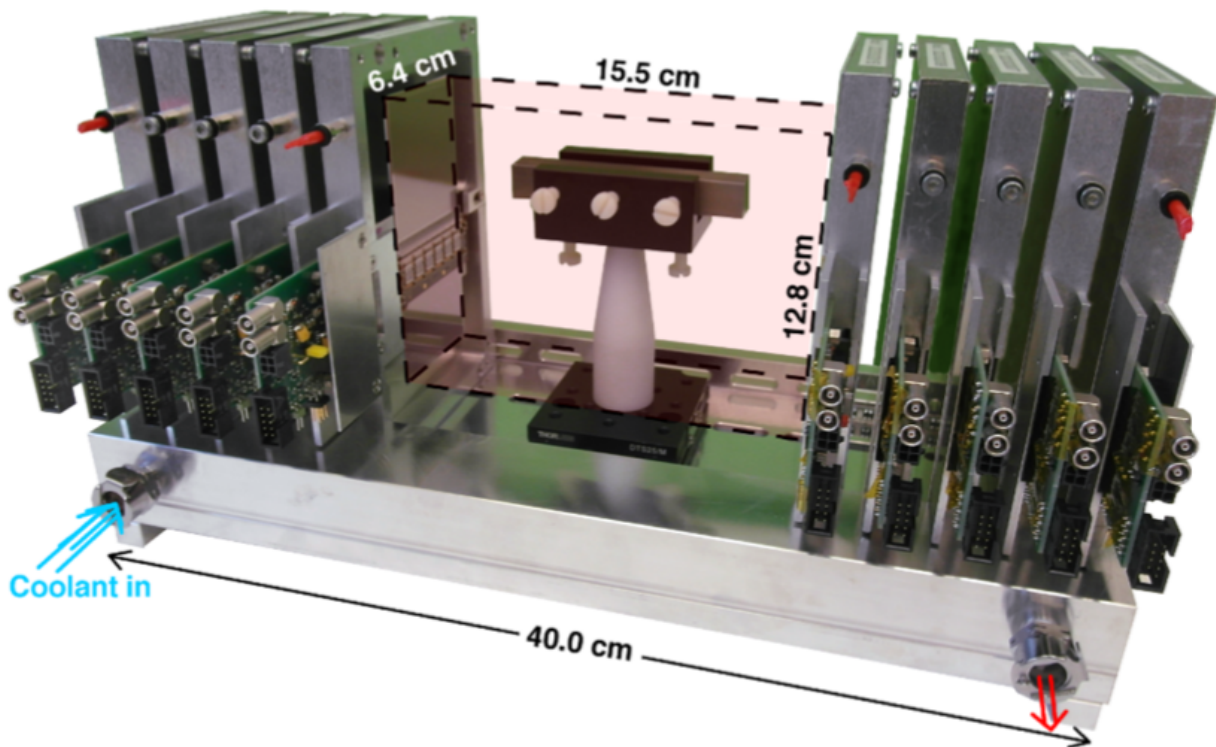


Figure 3: The aluminium support for cooling and alignment of the modules. The aluminium cover plate has been removed from one of the modules to display the silicon sensor. The imaging region between the tracking stations is marked in red containing a sample clamped to the plastic mount. This configuration is rotated by 90 degrees for cosmic muon data collection.

the module is designed to have low mass and radiation length [9]. Cooling is required to prevent thermal runaway and to reduce thermal noise, due to a power consumption of 6.0W per module. When unirradiated, the sensors are fully depleted at a reverse bias voltage of 150V.

The aluminium support in Fig. 3 cools and aligns the modules. The spacing between the modules on the support can be varied, allowing the tracker to be optimised for high resolution at large spacing or greater muon acceptance at small spacing. The aluminium surfaces are precision manufactured to around $20\mu\text{m}$ (a quarter of the silicon strip pitch), and ensure the modules are aligned and parallel. Two tracking stations, each containing four modules plus a spare, are mounted on the support. The module spacing is currently 23.8mm with a 155.2mm separation between the tracking stations. The support can lie flat for use in a particle beam, as seen in Fig. 3, or stand vertically if cosmic muons are chosen as a source.

Water coolant pumped at 10°C flows through the support at around $5 - 10\text{Lmin}^{-1}$ to dissipate heat from the modules. The modules are orientated such that the corner with the shortest thermal path to the sensors is in contact with the cold reservoir. The flat surfaces provide a good thermal contact even without thermal paste. The ATLAS upgrade temperature interlock is used to switch off the tracker when the temperature at the module hybrid exceeds 41°C or drops below 12°C . This avoids potential damage to the sensors due to thermal runaway, or condensation, in case of failure of the cooling system. The tracker is operated in an opaque box to reduce noise, which is flushed with nitrogen to avoid condensation on cold parts.

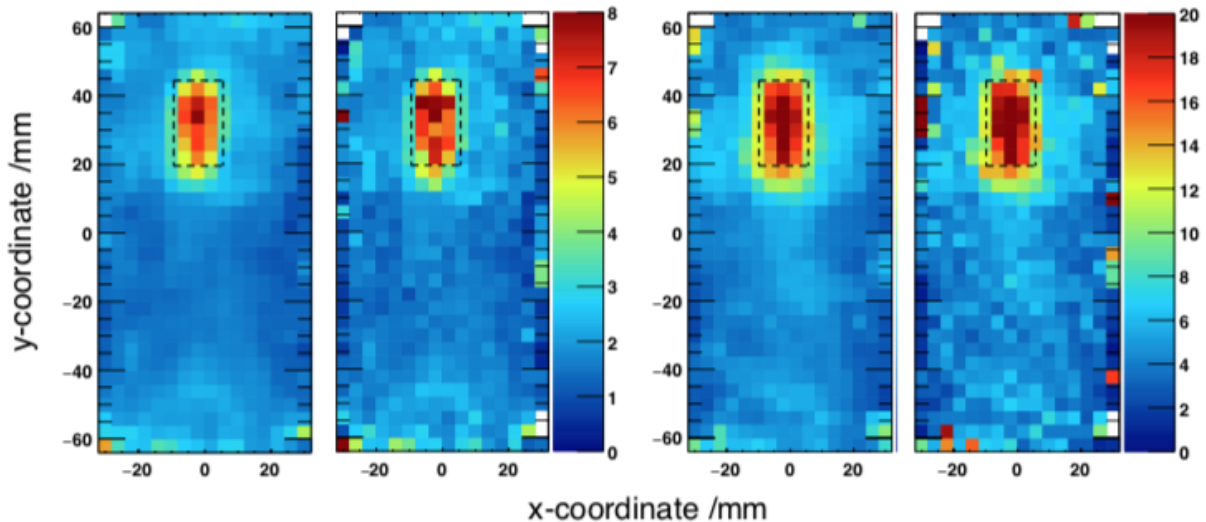


Figure 4: ASR of a lead sample with 45000 muons from experiment. The black dotted lines show the sample contours. From left to right: smoothed and non-smoothed ASR, for a 0.5 quantile and for a 0.8 quantile.

The system was found to be stable over weeks of data taking, with temperature fluctuations within 0.3°C and with a consistent trigger rate, efficiency of the silicon sensors and scattering angle resolution.

3.4 Reconstruction Techniques

The Angle Statistics Reconstruction (ASR) algorithm is currently implemented for the image reconstruction [11]. ASR is chosen as it is robust to changes in the system setup, easy to implement and has been shown to perform better than Point of Closest Approach (PoCA) algorithms [12]. PoCA algorithms suffer due to the low flux of muons which reduces the accuracy of Maximum Likelihood/Expectation Maximisation methods [13] [14]. The algorithm used in this report is the same as was used to analyse the data from the existing scanner in [3].

The algorithm defines a grid of voxels, 3-dimensional pixels, in the imaging region. For each event a score is generated, in this study the score is the absolute value of the scattering angle in the x-z plane. The incoming and outgoing muon trajectories are projected through the total volume. For each voxel, the distance between it and the point of closest approach of each of these projected trajectories is calculated. If the greater of these two distances is below a threshold distance, the event score is appended to a list associated with that voxel. This is repeated for each event. The result is a set of voxels each with a list of scores say N_j long. These lists are then sorted in ascending order and the $\lfloor qN_j \rfloor$ -th entry to the list, where the ‘quartile’ q is defined, is chosen as the final score for that voxel. Additional weightings from surrounding voxels are also implemented, there is more information available in [11]. The density assigned to a voxel is therefore calculated using its score, the scattering angle, and Equation. 1. Fig. 4 shows the effect of smoothing and quantile choice in the xy-projection of a $15 \times 25 \times 55\text{mm}^{-3}$ lead sample imaged using 45000 muons in the previous study. The algorithm performs well over a large range of quantiles, and can be adjusted to give the best contrast between the sample and background.

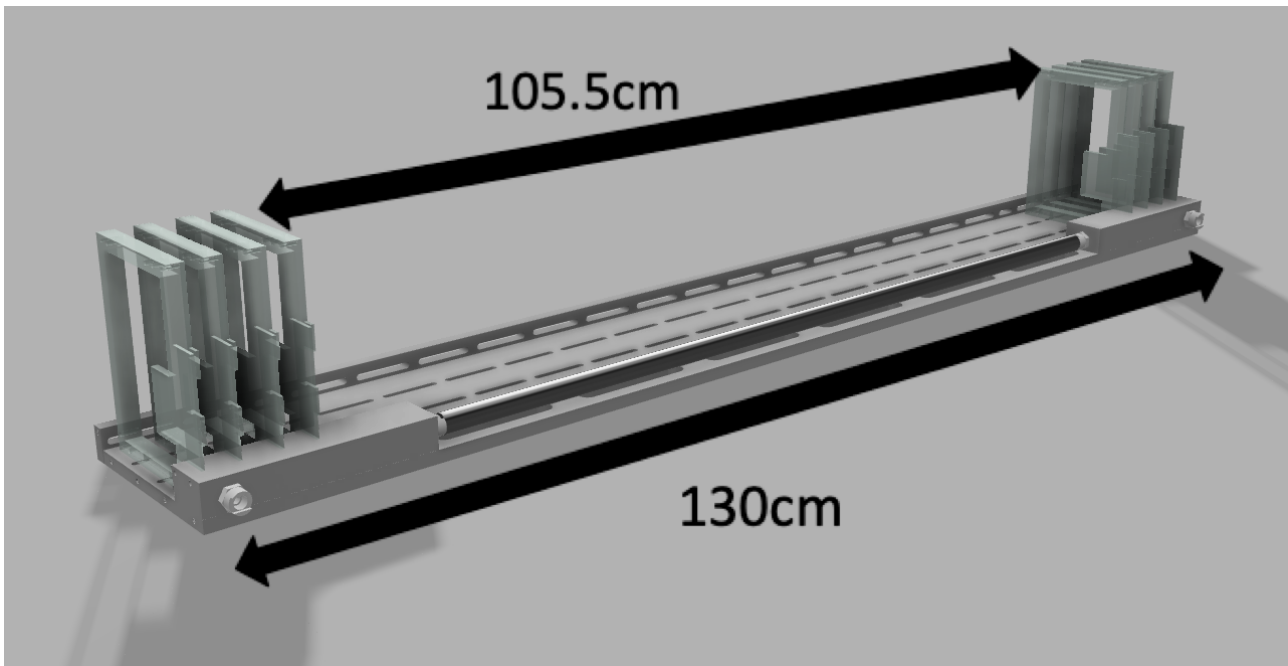


Figure 5: A 3D render (Fusion 360) of the new mechanical support. Pictured are the base plate, tension bar and cooling bar, arranged as if they were properly mounted. For context, the sensor handling frames, quarter-inch BSPT couplings and intermediary coolant pipe are depicted. The basic dimensions are displayed showing the total length (1300mm) and the distance between the tracking stations (105.5cm).

4 Scanner redesign

It was proposed that, in order to better understand the capabilities of commercial applications of muon scattering tomography, a prototype should be built that is capable of imaging an object with a thickness of about 100cm. This dimension is more representable of a typical architectural support structure such as a wall. The physical modifications designed and implemented are discussed in this section.

4.1 Mechanical Support

The main mechanical support, shown in Figure. 5, consists of a main baseplate to which a tension bar and cooling bar are secured. This forms a rigid structure onto which all the other components of the scanner are mounted. These pieces were redesigned to accommodate the new geometry, the technical drawings are given in the Appendix. They were constructed out of plough-ground Aluminium tooling plate, to be light weight yet rigid enough to survive the milling process and ensure a solid structure even when upright. They were also designed to have a tracking station separation of 105.5cm which can safely image an object of thickness 100cm. Threaded M5 screw holes are included in the edges of each piece, so that the structure can be secured to a perpendicular shelf if the extra stability is required.

The base plate, shown in Section 8.1, is a $1300 \times 175 \times 12\text{mm}^{-3}$ cuboid with slots and holes milled into it. The thin slots, shown on the left in the technical render, are used to secure the sensor handling frames and the sample holder. These have the same dimensions as in the previous design so that no changed to the bespoke handling frames was needed. The three slots at either end are designed such that the sensor spacing can be varied for optimisation, as discussed in Section 3.3, allowing a zero spacing stacking of the modules. The rest of aforementioned slots

are for mounting the sample. The thicker slots, shown on the right in the technical render, are for weight reduction. The holes in the face of the baseplate, either end of the weight reduction slots, are for securely mounting the cooling bars which will be discussed in further detail shortly. Threaded M5 screw holes run along one of the long edge, so that the tension bar can be secured.

The tension bar, shown in Section [8.2](#), adopts a similar design as in the existing scanner. The length has been increased to the new geometry and the mounting slots have been adjusted to align with the corresponding slots in the base plate. Holes are included to secure it to the base plate.

The design of the cooling bar is the most drastically modified and can be seen in Section [8.3](#). Cooling is only required at the sensors, not along the length of the sample. Hence the cooling bar was split into 2 halves, to be connected by an insulated plastic pipe similar to that providing the input and output stream. This also saves on material cost and unnecessary weight. To avoid bottlenecking and ensure a uniform flow, four threaded, quarter-inch BSPT, brass straight hose couplings are fixed onto the cold bar, two on each half. These act as the coolant inlet and outlet as well as the connection of the two halves. A channel was also cut to house a rubber o-ring to provide a good seal when screwing into the base plate. The flat surfaces should provide a good thermal contact and no thermal paste was required for the previous scanner. When in the vertical arrangement, the top coupling should be used as the inlet, so that gravity assists the passage of water through the system. The success of this bar would be assessed by its ability to maintain the temperature of the modules in the acceptable region of 12 – 41°C with fluctuations within 0.3°C. A performance previously achieved allowing for successful imaging [\[3\]](#).

4.2 Light tight Environment

Due to the length of the new scanner, 1300mm, a cheap commercial alternative to the current Kängabox® was not found. It was initially thought that stacking two of these boxes might provide a solution, however, as the box must also house the triggering scintillators and potentially a support shelf to mount the support to, this would also not be large enough. Therefore it is suggested that a bespoke case is constructed, potentially out of a light insulating material such as sandwich board, that can properly house the scanner. The same patch panel can be repurposed for this new box to ensure a light-tight connection for the wiring and coolant. The existing patch-panel accommodates all the required wiring. This is a re-design that ideally requires access to physical pieces and so was not explored further in this report. It is suggested that, alternatively, two small light tight environments could be built around each tracking station respectively. This would require a second nitrogen gas line but would reduce the amount of material and also provide a protective layer between the sample and the sensors. The sample is not required to be in a light tight environment and the relatively low radiation length of the material shouldn't account for a significant drop in performance, but again this has not been explored in the scope of this report.

4.3 Internal wiring

As part of the preparation for disassembling and reassembling the prototype scanner, the wiring, voltages, cooling and monitoring systems were all thoroughly checked in the existing scanner. Notes were made so that an identical set-up could be recreated with the new geometry. Very few wiring adjustments need to be made. The power supply to the two tracking stations is currently daisy chained together, however there are wires available to provide power to them separately.

The control boards for the two tracking stations are currently bolted together. These should be separated in the new configuration so that the same short serial data strip-cables can be used. This will require them to be powered separately or for a longer cable to daisy chain them together. The rest of the wiring should be left as it is.

The existing scanner was then turned on and the operating software was set up to allow for a scan to be made. In the process it was observed that one of the silicon sensors was quickly getting hotter than the rest. This sensor reached 41°C and triggered the temperature interlock system, turning off the whole scanner after only about 5 minutes of operation. The cause of this misbehaviour was not diagnosed and so the module was disabled until the problem gets resolved, to avoid any further potential damage. Data was recorded correctly, however the scanner was not run for long enough to get any statistically significant results.

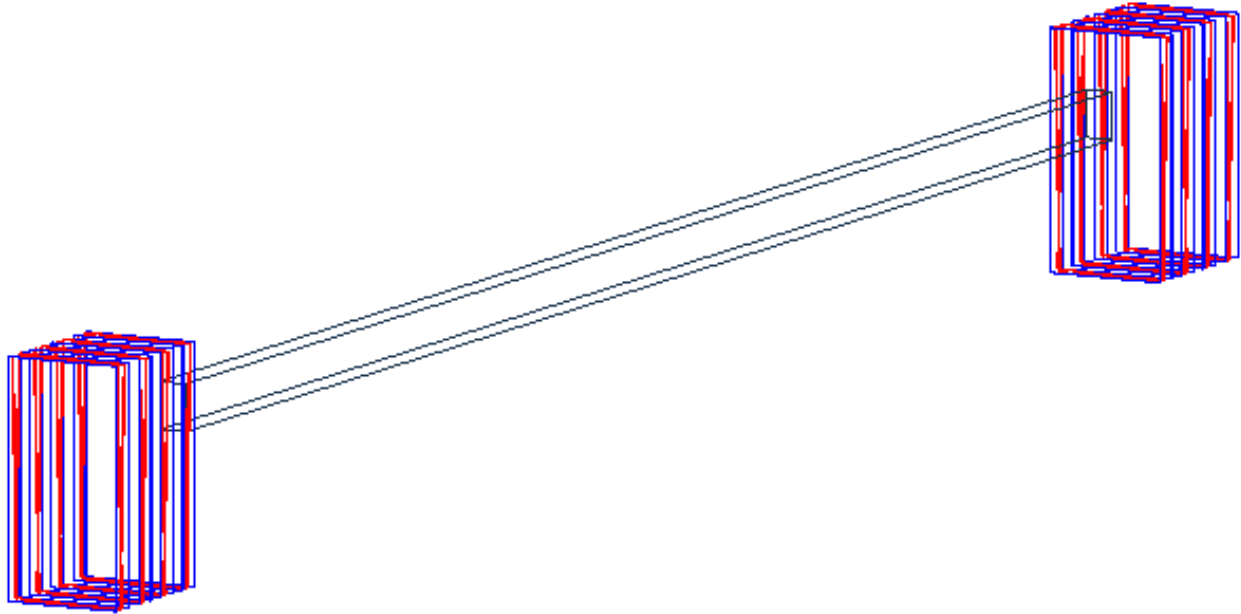


Figure 6: Geant4 simulation of the modified tracker. The silicon sensors are drawn in red at a stereo angle with the aluminium covers drawn in blue. The sample is drawn in black and was only present in the imaging run in Section.5.2

5 Simulation and Analysis

To supplement the physical redesign of the prototype scanner, the calibration and reconstruction software was also modified to accommodate the new geometry. To get an appreciation for how these modifications will effect the performance of the reconstruction techniques some data was required to pass through the software. Thus, in the absence of the physical scanner, a simulation was constructed using Geant4 to generate such data. The specifics of the simulation are discussed in Section.5.1 . The results of the reconstruction techniques are discussed in Section.5.2 and Section.5.3 for simulations without and with a sample respectively.

5.1 Geant4 detector description

A Geant4 description of the prototype MST tracker in its state before this project began was developed to help understand the limitations on the angular resolution and track quality of the detector. This description was modified in accordance with the modifications described in Section. 4 and can be seen in Fig. 6. The geometry of the scanner is simulated by virtual sensor modules in air. These have a random Gaussian offset in the x axis, perpendicular to the long axis, with a standard deviation of $80\mu\text{m}$ and a rotation in the xy plane of 3mrad . The silicon sensors were designed to contribute only 1.17% of the total radiation length when averaged over each sensor [15], so that significant scattering did not occur in them. The 1mm thick aluminium sensor covers positioned either side of the sensor contribute 1.12% of the radiation length. The spatial resolution of each sensor is modelled by assigning each hit to the center of an $80\mu\text{m}$ strip. The mechanical support, readout chips, triggering scintillation and cooling is not included in the description. The simulation outputs silicon sensor positional data in the same format as the experimental data output. This means that the results produced by this simulation can be passed through the calibration and image reconstruction analysis software in the same way as actual experimental data. The positions of the silicon sensors were changed to reflect the modifications made to the scanner. The new positions of the silicon are given in

z coordinate [mm]			
Tracking station 1		Tracking station 2	
1	$-(566.46 + 23.8)$	9	535.90
2	$-(566.46 + 23.8 - 2.8)$	10	$535.90 + 2.8$
3	-566.46	11	559.81
4	$-(566.46 - 2.8)$	12	$583.19 + 2.8$
5	-542.82	13	$559.81 + 2.8$
6	$-(542.82 - 2.8)$	14	583.19
7	-519.10	15	$583.19 + 23.8$
8	$-(519.10 - 2.8)$	16	$583.19 + 23.8 + 2.8$

Table 1: The z coordinates of the silicon sensors with respect to the center of the tracker description. There are 2 sensor strips per module, separated by 2.8mm and each module is separated by approximately 23.8mm. The two tracking stations are separated by 105.2cm.

Table [1](#).

The cosmic ray muons are generated in a plane centred on and normal to the long axis of the tracker. This plane has an area of $3.3 \times 6.63\text{cm}^{-2}$ and is positioned 9.74mm from the first silicon sensor (a z coordinate of -600.0mm for reference with Table [1](#)). Muons generated outside of this region cannot pass through both tracking stations. As this simulation is not aimed to analyse the rate of imaging, such events would be discarded and lower the reconstruction statistics. The silicon sensors are modelled to operate at an efficiency of 90% where $\approx 5.3\%$ of the events resulted in a track. The angular and energy distributions of the muons is sourced from [\[16\]](#).

The sample is modelled as an iron cuboid, suspended in air with a long axis dimension of 100cm and a cross-sectional area of $1.5 \times 2.5\text{cm}^{-2}$. The sample is centred between the two tracking stations, but off-set from the origin in the x and y axes. The sample was activated by selecting muons as the simulated particle, and deactivated by selecting non interacting ‘geantinos’ as the simulated particle. The geometry was the geometry suggested in the project proposal and should provide a strong test for the integrity of the reconstruction algorithms.

5.2 Scattering angle resolution

The simulation was run generating 10 million muons, the properties of which were taken from the distributions outlined above. This was run without a sample present resulting in 525764 tracks, 472543 of which hit the second tracking station. The reconstruction software identified 18795 scattering events. The simulation took around 10 hours to run, and the reconstruction took about 2 hours.

The distribution of scattering angles is displayed in Fig. [7](#). A mean of 1.147mrad is observed in the x-direction, with one standard deviation of 2.3mrad. The expected mean should be zero from the theory, as is the case for the y-direction scattering angles. This is currently not explained. However, a detailed calibration stage is performed in the reconstruction techniques which was not adapted for the new geometry due to time constraints, it is highly probable that this is introducing some bias. The width arises from internal scattering in the modules. It was found in the short baseline simulation that this width varied from $0.9 - 7.9\text{mrad}$ depending on the energy of the muons [\[3\]](#) and so this value seems reasonable for the chosen energy distribution.

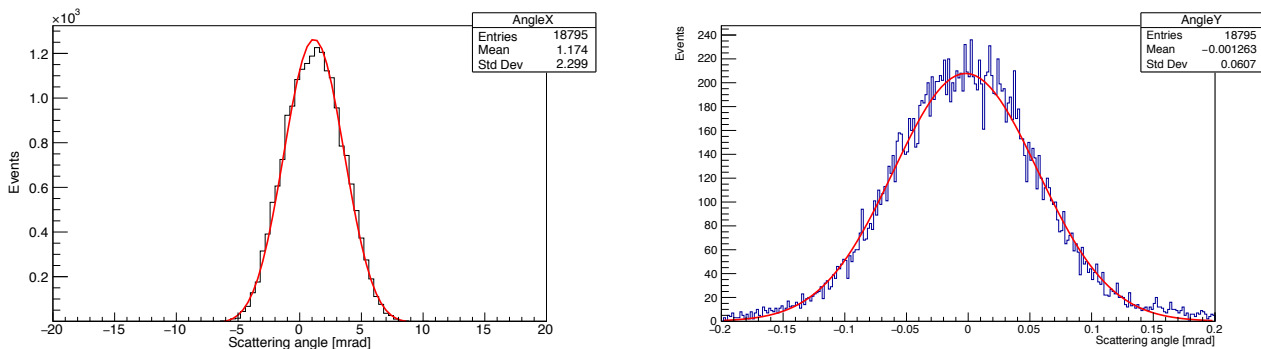


Figure 7: Scattering angular distribution of a simulation of 10 million muons through the new scanner geometry in the absence of a sample. The red line shows a Gaussian fit to this data. The left and right plots show the scattering angle in the x and y direction respectively.

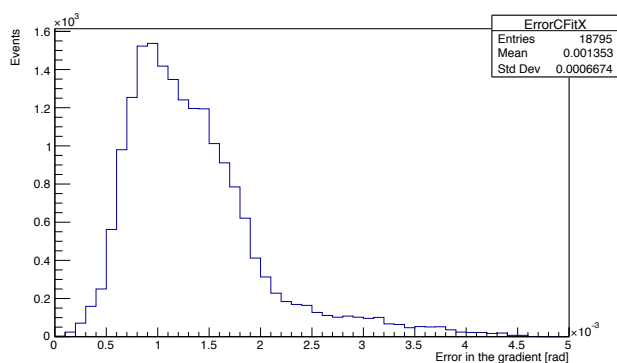


Figure 8: The error in the gradient of a straight line fit through the hits in the sensors from the simulation in the absence of a sample.

The error associated with the scattering angle is estimated using the error in the gradient of a straight line fitted to the hits in the silicon sensors [17]. This is evaluated for the even and odd sets of silicon layers and the results are combined in quadrature. The results of this for the simulation are shown in Fig. 8. The peak occurs at a value of less than 1mrad which displays a similar error as in the short baseline simulation. This is to be expected because the simulations are identical as the muon passes through the tracking station. The width of the peak is also similar to that of the 90% efficient short baseline simulation.

The distribution obtained through experiment in the short-baseline configuration displayed a larger standard deviation and a larger error in the gradient than the equivalent simulation [4]. This was attributed to misalignments left uncorrected by calibration, or to uncertainty in cluster assignment due to detector noise or cross talk. It can be expected that a similar discrepancy will be observed when experimental data is obtained in the new configuration.

5.3 Image reconstruction

The simulation was run again generating 10 million muons in the same configuration as used for the angle resolution experiment. However in this experiment the sample was activated so the imaging capability of the reconstruction could be assessed. A random sample of 7 trajectories is displayed in the Appendix, Section 8.4. Of the 10 million muons 443205 tracks were

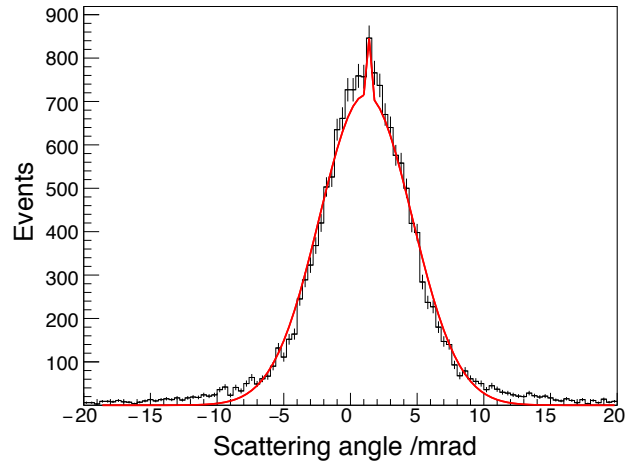


Figure 9: Scattering angular distribution of a simulation of 10 million muons through the new scanner geometry with a sample present. The red line shows a Gaussian fit to this data.

detected, with 390918 hitting the second tracking station. This simulation took 40 hours to run. The reconstruction algorithm took the same amount of time as it took without a sample as expected, returning 17116 scattering events.

From the angular distribution, [9](#), a similar offset of the mean is displayed which is assumed to be caused by the same error in the simulation without a sample. However a spike is also seen at non-zero value, which does not conform to the Gaussian fit. This is attributed to the increased scattering due to the sample. Unfortunately an image was not reconstructed by the ASR algorithm. This was not explored further.

It is suggested that in future studies the range of angles the simulated muons are generated is restricted to be more parallel to the long axis of the detector. This will increase the statistics of the scattering events and may help in refining the reconstruction process.

6 Conclusion

The prototype Muon Tomography Scanner was redesigned to accommodate a sample of length 100cm. A new mechanical support and cooling system was developed with a proposed success criteria of maintaining the temperature of the modules in the acceptable region of 12 – 41°C with fluctuations within 0.3°C. These pieces were commissioned out of plough-ground aluminium tooling plate and the technical drawings are given in the Appendix.

It was observed that one of the silicon sensors was generating a significant amount of heat, triggering the temperature interlock system to shut down the tracker after only about 5 minutes. The cause of this was not diagnosed and so this module was disconnected to prevent any further damage.

A Geant4 simulation of the new detector geometry was designed and run. 10 million muons were generated and passed through the detector both with a sample present and a sample absent. The output of this was then passed through the reconstruction software. In the absence of a sample distributions of the scattering angle and error in the gradient were generated over 12 hours. The scattering angle displayed a mean of 1.147mrad and a width 2.3mrad. The width is reasonable however the non-zero mean is not expected and is likely a result of the calibration performed on the simulated data. The error in the gradient displayed a mode of less than 1mrad and a width in accordance to the simulation performed in the short baseline simulation as expected. These results show that there is more work that needs to be done on the reconstruction software before it is ready to analyse experimental data. The simulation with the sample took 40 hours to run and so perhaps if this simulation is to be used further it should be parallelised to reduce the run time. A deviation from a Gaussian scattering distribution was observed believed to be due to the presence of the sample, however an image was not formed.

The future of this project lies in the construction of the new prototype. Assembly of the mechanical support should allow for the details of the light-tight environment to be finalised. It should also then be checked for leaks before transferring the silicon sensors to the new geometry. A test of the performance of the cooling system should be conducted before any extended use is conducted. A proper amount of time should be dedicated to assessing why the simulation results have a non zero mean, which may require parallelising the simulation.

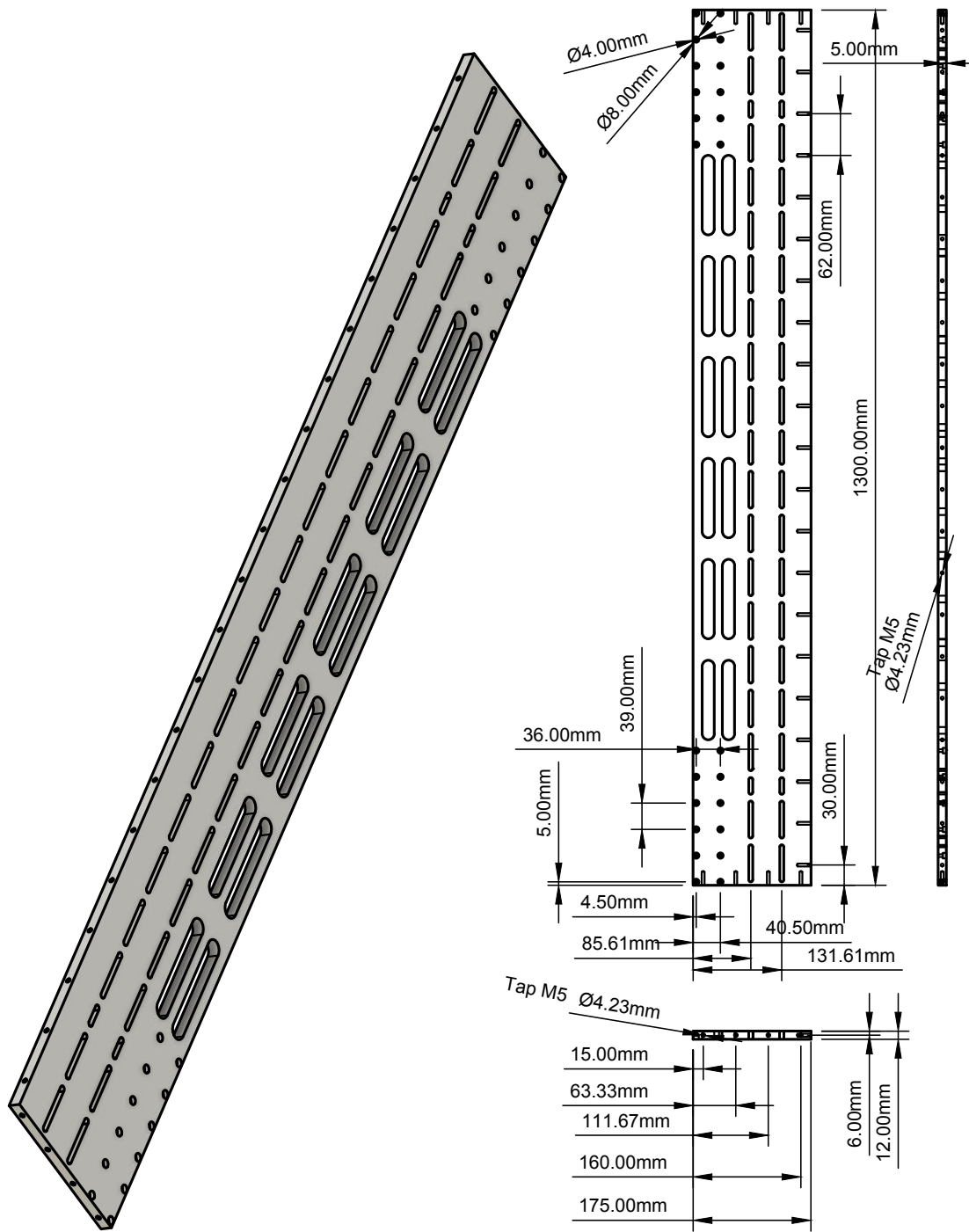
7 References

- [1] William C. Friedhorsky et al. “Detection of high-Z objects using multiple scattering of cosmic ray muons”. In: *Review of Scientific Instruments* 74.10 (2003), pp. 4294–4297. DOI: [10.1063/1.1606536](https://doi.org/10.1063/1.1606536), eprint: <https://doi.org/10.1063/1.1606536> URL: <https://doi.org/10.1063/1.1606536>.
- [2] Bertram Schwarzschild. “Cosmic-Ray Muons Might Help Thwart Transport of Concealed Fissile Material”. In: *Physics Today* 56.5 (2003), pp. 19–22. DOI: [10.1063/1.1583524](https://doi.org/10.1063/1.1583524), eprint: <https://doi.org/10.1063/1.1583524> URL: <https://doi.org/10.1063/1.1583524>.
- [3] F. Keizer et al. “A compact, high resolution tracker for cosmic ray muon scattering tomography using semiconductor sensors”. In: *Journal of Instrumentation* 13.10 (Oct. 2018), P10028–P10028. DOI: [10.1088/1748-0221/13/10/p10028](https://doi.org/10.1088/1748-0221/13/10/p10028) URL: <https://doi.org/10.1088/1748-0221/13/10/p10028>.
- [4] Floris Keizer. “Sub-nanosecond Cherenkov photon detection for LHCb particle identification in high-occupancy conditions and semiconductor tracking for muon scattering tomography”. Presented 04 Oct 2019. June 2019. URL: <http://cds.cern.ch/record/2699823>.
- [5] J. Burns et al. “A drift chamber tracking system for muon scattering tomography applications”. In: *Journal of Instrumentation* 10.10 (Oct. 2015), P10041–P10041. DOI: [10.1088/1748-0221/10/10/p10041](https://doi.org/10.1088/1748-0221/10/10/p10041) URL: <https://doi.org/10.1088/1748-0221/10/10/p10041>.
- [6] Peter K.F. Grieder. Amsterdam: Elsevier, 2001. ISBN: 978-0-444-50710-5. DOI: <https://doi.org/10.1016/B978-044450710-5/50003-8>.
- [7] C. Patrignani et al (Particle Data Group). “Cosmic Rays”. In: *Chin. Phys. C* 40 (2017), p. 100001. URL: <http://pdg.lbl.gov/2017/reviews/rpp2017-rev-cosmic-rays.pdf>.
- [8] H. A. Bethe. “Molière’s Theory of Multiple Scattering”. In: *Phys. Rev.* 89 (6 Mar. 1953), pp. 1256–1266. DOI: [10.1103/PhysRev.89.1256](https://doi.org/10.1103/PhysRev.89.1256) URL: <https://link.aps.org/doi/10.1103/PhysRev.89.1256>.
- [9] Gerald R. Lynch and Orin I. Dahl. “Approximations to multiple Coulomb scattering”. In: *Nuclear Instruments and Methods in Physics Research Section B: Beam Interactions with Materials and Atoms* 58.1 (1991), pp. 6–10. ISSN: 0168-583X. DOI: [https://doi.org/10.1016/0168-583X\(91\)95671-Y](https://doi.org/10.1016/0168-583X(91)95671-Y) URL: <http://www.sciencedirect.com/science/article/pii/0168583X9195671Y>.
- [10] S. Eidelman et al. “Passage of particles through matter”. In: *Review of particle physics* B (592 2004). URL: <http://pdg.lbl.gov/2004/reviews/passagerpp.ps>.
- [11] M. Stapleton et al. “Angle Statistics Reconstruction: a robust reconstruction algorithm for Muon Scattering Tomography”. In: *Journal of Instrumentation* 9.11 (Nov. 2014), P11019–P11019. DOI: [10.1088/1748-0221/9/11/p11019](https://doi.org/10.1088/1748-0221/9/11/p11019) URL: <https://doi.org/10.1088/1748-0221/9/11/p11019>.
- [12] L.J. Schultz et al. “Image reconstruction and material Z discrimination via cosmic ray muon radiography”. In: *Nuclear Instruments and Methods in Physics Research Section A: Accelerators, Spectrometers, Detectors and Associated Equipment* 519.3 (2004), pp. 687–694. ISSN: 0168-9002. DOI: <https://doi.org/10.1016/j.nima.2003.11.035> URL: <http://www.sciencedirect.com/science/article/pii/S0168900203028808>.
- [13] G. Wang, L. J. Schultz, and J. Qi. “Bayesian Image Reconstruction for Improving Detection Performance of Muon Tomography”. In: *IEEE Transactions on Image Processing* 18.5 (May 2009), pp. 1080–1089. ISSN: 1941-0042. DOI: [10.1109/TIP.2009.2014423](https://doi.org/10.1109/TIP.2009.2014423).

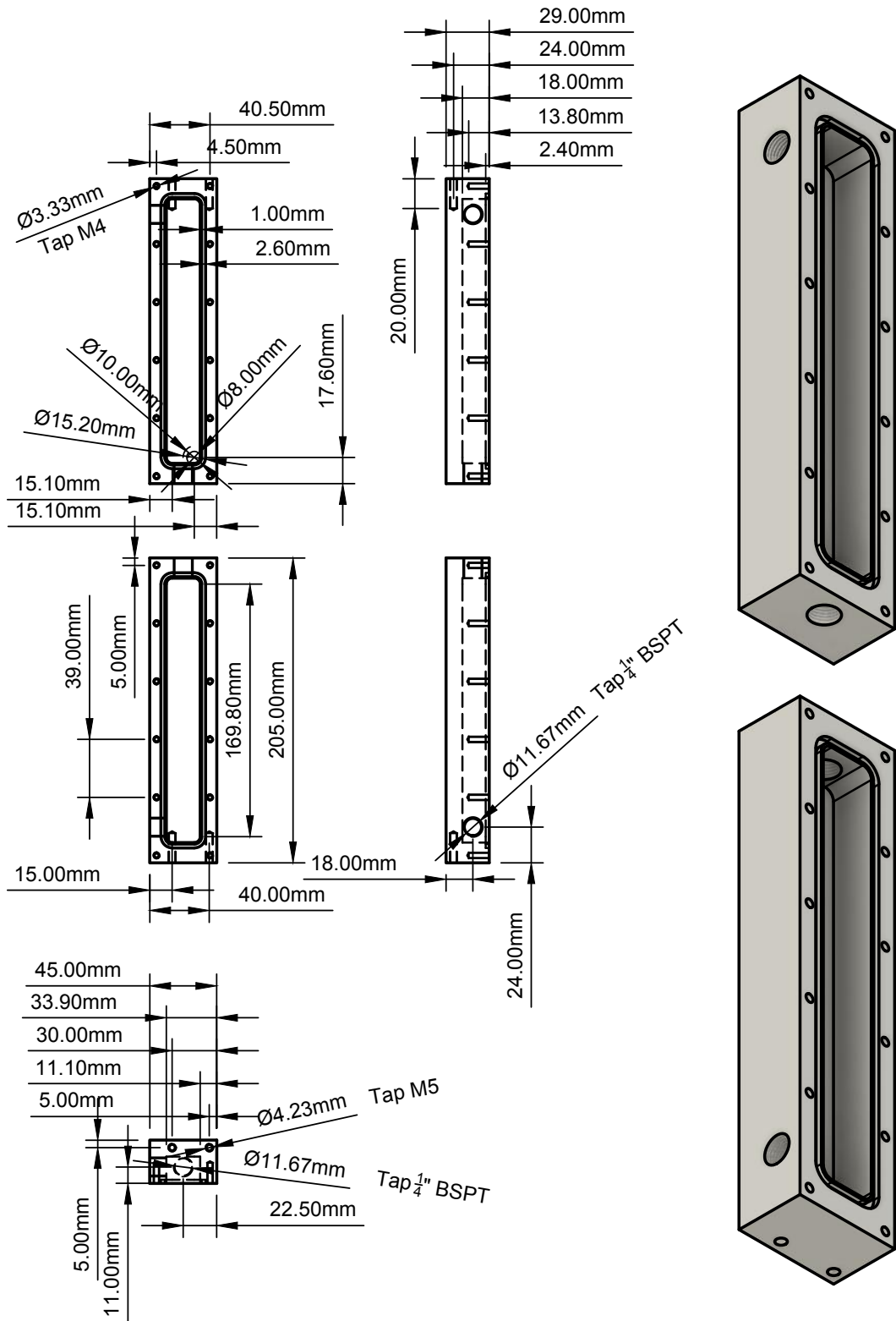
- [14] G. Wang, L. Schultz, and J. Qi. “Statistical Image Reconstruction for Muon Tomography Using a Gaussian Scale Mixture Model”. In: *IEEE Transactions on Nuclear Science* 56.4 (Aug. 2009), pp. 2480–2486. ISSN: 1558-1578. DOI: [10.1109/TNS.2009.2023518](https://doi.org/10.1109/TNS.2009.2023518).
- [15] A. Abdesselam et al. “The barrel modules of the ATLAS semiconductor tracker”. In: *Nuclear Instruments and Methods in Physics Research Section A: Accelerators, Spectrometers, Detectors and Associated Equipment* 568.2 (2006), pp. 642–671. ISSN: 0168-9002. DOI: <https://doi.org/10.1016/j.nima.2006.08.036>. URL: <http://www.sciencedirect.com/science/article/pii/S016890020601388X>.
- [16] S. Chatzidakis, S. Chrysikopoulou, and L.H. Tsoukalas. “Developing a cosmic ray muon sampling capability for muon tomography and monitoring applications”. In: *Nuclear Instruments and Methods in Physics Research Section A: Accelerators, Spectrometers, Detectors and Associated Equipment* 804 (2015), pp. 33–42. ISSN: 0168-9002. DOI: <https://doi.org/10.1016/j.nima.2015.09.033>. URL: <http://www.sciencedirect.com/science/article/pii/S0168900215010888>.
- [17] G. L. Squires. *Practical Physics*. 4th ed. Cambridge University Press, 2001. DOI: [10.1017/CB09781139164498](https://doi.org/10.1017/CB09781139164498).

8 Appendix

8.1 Technical Drawing of Base Plate



8.3 Technical Drawings of Cooling Channel



8.4 Simulation with some trajectories displayed

